# A Parallel Disc Device for studying corrosion under intense flow conditions

**N. Subaschandar, J.N. Connor, A.V. Deev, I.R. McNeilly and D. Druskovich**

Process Engineering and Light Metals Centre
Central Queensland University, Gladstone, Queensland, 4680 AUSTRALIA

## Abstract

A novel electrochemical Parallel Disc Device (PDD) has been designed and built at the Process Engineering and Light Metals (PELM) Centre of Central Queensland University. This device, built primarily to study aspects of flow accelerated corrosion, consists of two discs separated by a precision controlled gap. The bottom disc (which accommodates the working electrode) is immobile while the top disc rotates and enables a flow of liquid between the discs. The gap between the discs can be set within the range 0.050 to 5.000 mm with a precision of 0.005 mm. The PDD is capable of generating very high wall shear rates and the shear of liquid at the working electrode is purely tangential as long as flow between the discs remains laminar.

This paper presents results of preliminary Computational Fluid Dynamics (CFD) characterisations of the fluid flow in the gap between the parallel discs. In addition we present some results for the electrochemical reduction of dissolved oxygen at a copper PDD electrode.

Keywords: parallel disc device, flow accelerated corrosion, wall shear rate, computational fluid dynamics, electrochemical reduction of oxygen.

*corresponding authors: a.deev@cqu.edu.au and d.druskovich@cqu.edu.au

## Introduction

In industrial process plants it is often observed that high fluid flow rates may result in flow enhanced corrosion of steel surfaces. However, due to the inherent difficulties in measuring corrosion rates in the plant environment we often need to resort to rapid laboratory tests to get an estimate of this important parameter [1].

The generally accepted approach for laboratory corrosion testing in flowing liquids is to use simple geometries that generate predictable flow that can be related to fluid- flow in complex plant situations. Common laboratory geometries include the rotating disc, rotating cylinder and the impinging jet technique [1]. Although these techniques can model flow for a wide range of fluid velocities, only rarely do they permit quantitative modelling of plant corrosion rates [2, 3]. The obstacles to improving the accuracy of corrosion testing data are inherently a consequence of the very complex nature of turbulent flow. However, there is a real demand for corrosion testing under very severe flow conditions with Reynolds numbers of the order of $10^7$ and wall shear rates as high as $10^5$ to $10^7$ $s^{-1}$. It has been widely accepted that both wall shear stress and mass transfer coefficient are key parameters when investigating the condition of similarity between laboratory corrosion data and corrosion in the plant environment [4]. In 2005 we reported a Parallel Disc Device (PDD) that allows the generation of high wall shear rates, while maintaining laminar flow conditions [5].

A schematic of the device is shown in Fig.1. The PDD consists of two discs (**1** and **2**) separated by a precision controlled gap distance, *b*. The top disc has a diameter of 80 mm and it can be rotated by a DC motor capable of speeds up to 10,000 rpm through a tooth belt driving a pulley (**3**). The bottom disc is immobile and incorporates the test (or working) electrode (**4**). The gap distance can be set by the operator within the range 0.050 to 5.000 mm, with an estimated precision of $\pm$ 0.005 mm. This precision is made possible by two coaxial columns (**5** and **6**) sliding inside each other. Precision nuts (**7** and **8**) fix the relative position of the columns, which in turn fixes the gap distance. The device assembly is rigidly held together by three support columns (**9**).

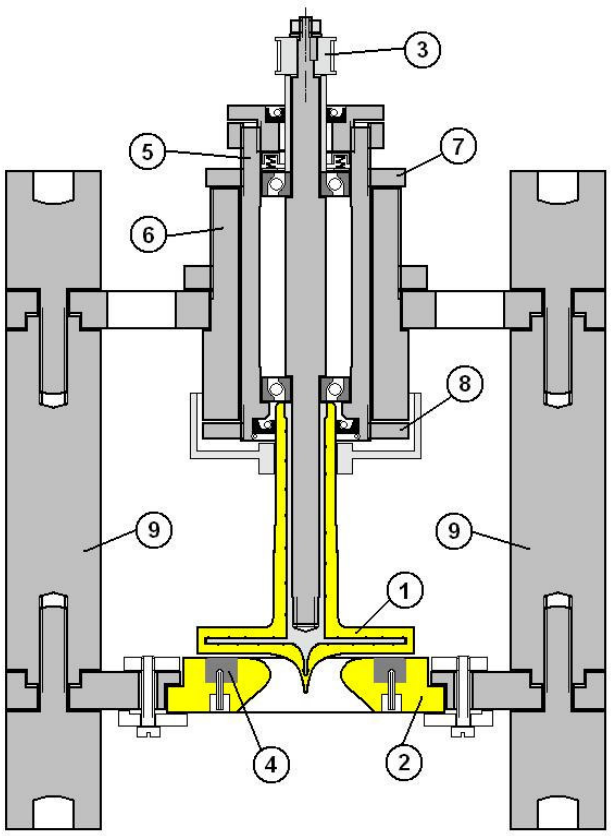


Figure 1. Schematic of Parallel Disc Device (PDD).

To estimate the Reynolds number for the flow in the gap between the discs ($Re_{PDD}$) the gap width $b$ was chosen as a characteristic length and the circumferential velocity at the surface of the rotating disc ($2\pi \cdot r \cdot \omega$) was chosen as a characteristic velocity:

$$\mathrm{Re}_{PDD} = \frac{2\pi \cdot r \cdot \omega \cdot b}{\nu} \quad , \qquad (1)$$

where $r$ is the radius of the top disc (40 mm), $\omega$ is the angular velocity and $\nu$ is the kinematic viscosity of water. Fig. 2 shows $Re_{PDD}$ as a function of rotation speed (rpm) for the gap widths of 0.100 mm and 0.250 mm.

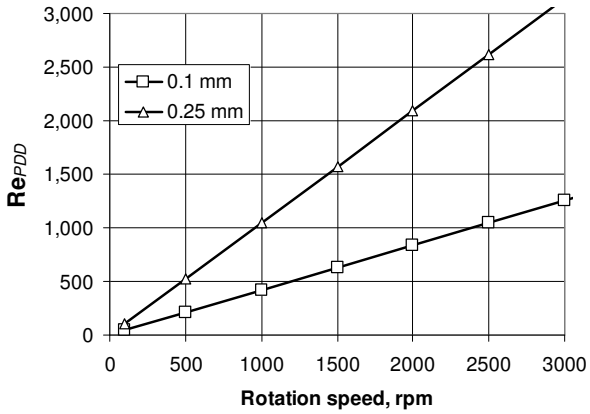


Figure 2. Calculated Reynolds numbers for the PDD as function of rotation speed at two gap distances, 0.100 and 0.250 mm.

This figure illustrates that at rotation speeds not exceeding 1,500 rpm the risk of the onset of the turbulent flow regime in the gap of the PDD is low for both gap dimensions.

Although the use of the parallel disc arrangement is not new in flow accelerated corrosion studies (see, for example, references [6] and [7]), fluid flow at the working electrode for the devices developed by other researches was distinctly turbulent. The device presented here has laminar flow in the gap between the discs and it is this feature that makes it unique.

In this paper we summarise key aspects of the computational fluid dynamics (CFD) characterisation of the PDD as well as the results of some electrochemical investigations conducted with this device.

## Computational Study

Flow visualization for the PDD is particularly difficult because of the very small gap dimension between the discs. Thus, an attempt was made to characterise the fluid flow for the device using computational fluid dynamics techniques. The CFD modelling approach allows generation of a vast number of parameters relating to flow behaviour for a system, which would be very difficult in an experimental study. It should be noted however, that the validation of the CFD model developed can be done to a limited extent only, due to the lack of experimental data for the flow in such narrow gaps between the discs. At the same time, the analytical von Karman solution for flow over a single rotating disc (RD) is readily available [8]. That is why the flow over a single rotating disc was also modelled in this work. The CFD settings for the RD model were similar to those for the PDD model, and the computational data generated for the RD were validated using that analytical solution.

The modelling for this study was done using the commercially available CFD software FLUENT ver. 6.2.16. For the single rotating disc the computational domain was set up as a 3-dimensional model. A 2-dimensional axisymmetric model was developed for the PDD because of the vast computing requirements for this geometry. GAMBIT ver. 2.3.16 was used to construct and mesh the computational domain for both the RDE and the PDD. A schematic of the computational domain for the PDD is shown in Fig. 3. The computational model for the RD is similar to that for the PDD, except for the fact that the RD has no bottom disc and that it was constructed in a three-dimensional domain. The geometries constructed for the present CFD analysis are simplified models of the actual geometries. The computational domain for the RD had approximately 326,000 cells and 340,000 nodes, while there were 1,600,000 cells and 827,000 nodes for the PDD set at a 0.250 mm gap and 2,050,000 cells and 1,050,000 nodes for a 0.100 mm gap. The rotational speed of the rotating disc was varied from 100 to 1,500 rpm. Water was used as the working fluid and flow was assumed to be laminar.

## Results and Discussion

### Single Rotating Disc Modelling

A 3-dimensional model was generated for this well characterized system. Fig. 4 compares the computed velocity components with the analytical von Karman solution [8]. The excellent agreement validates the model used.

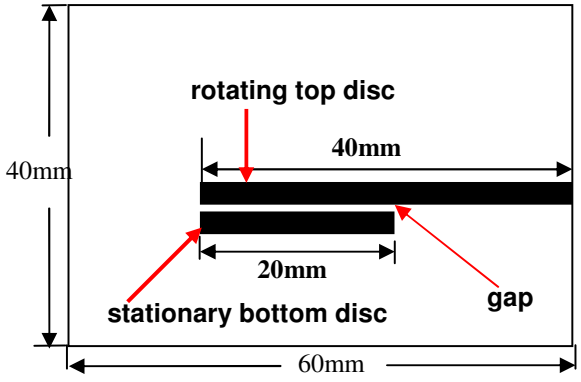


Figure 3. A schematic of the computational domain for the PDD (due to axisymmetry only half the disc was modelled).

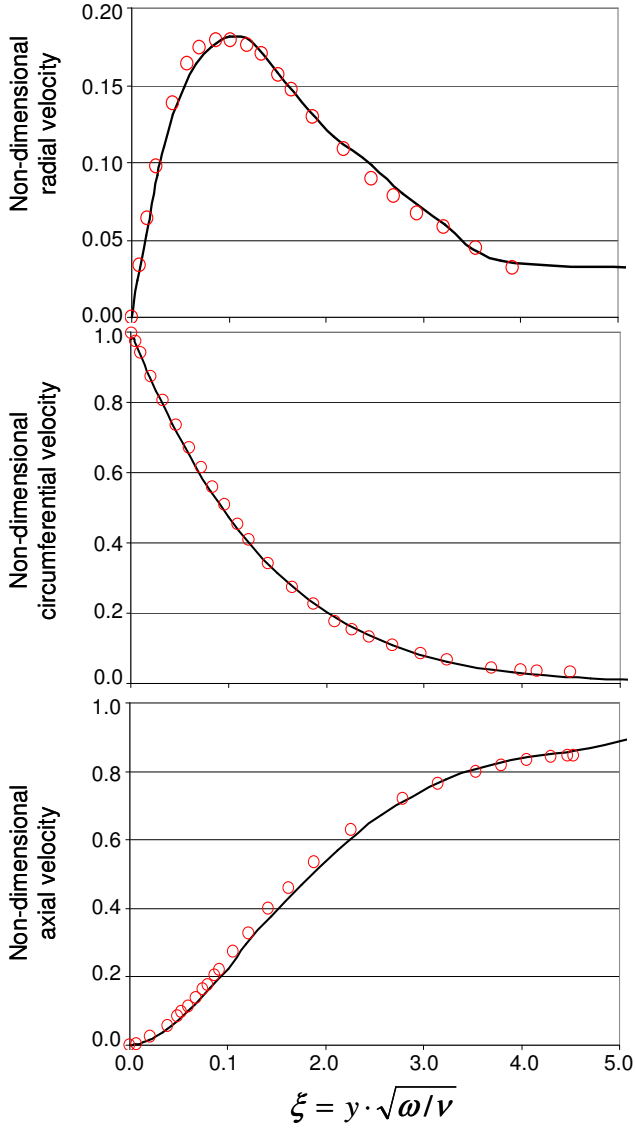


Figure 4. The CFD computed velocity components (open circles) compared to the von Karman mathematical solution (solid line) for a single rotating disc: (a) the non-dimensional radial velocity, (b) the non-dimensional circumferential velocity, (c) the non-dimensional axial velocity. The horizontal axis represents a non-dimensional distance $\xi$ from the bottom disc (*Y*-axis is normal to the disc surface).

## PDD Modelling

A contour plot of the velocity magnitude in the computational domain for a gap distance of 0.250 mm and a rotational speed of 1,000 rpm is shown in Fig. 5. Instability can be observed at the outer rim of the rotating disc (this is also observed experimentally). Similar flow patterns were observed for a PDD with a gap of 0.100mm at a rotational speed of 1,000 rpm.

Flow within the gap between the discs exhibited complex behaviour. For both 0.100 and 0.250 mm gaps, at all the rotational speeds in the range studied here, the flow was attached to both walls almost throughout the entire length of the gap. However, for 0.250 mm gap some reverse flow at the surface of the immobile bottom disc could be observed within a small (~ 5 mm long) region near the outer rim of the discs. This reverse flow diminished as the gap distance was reduced and no reverse flow was observed for a gap of 0.100 mm.

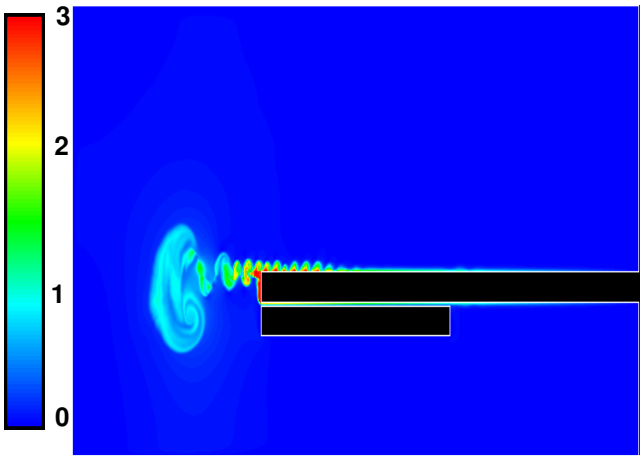


Figure 5. Contours of velocity magnitude (m/s) in the PDD computational domain. Gap = 0.250 mm and rotation speed = 1,000 rpm.

Fig. 6 shows the velocity vectors inside the gap and near the outer edge of the discs for both 0.250mm and 0.100mm gaps. The pictures relate to small, approximately 20 and 50 μm wide regions, adjacent to the stationary disc for gaps of 0.100 and 0.250 mm, respectively. Fig. 6(a) indicates that for a gap of 0.250 mm there is a reverse flow at the surface of immobile disc close to its outer edge, while for the gap of 0.100 mm the reverse flow does not occur (Fig. 6(b)).

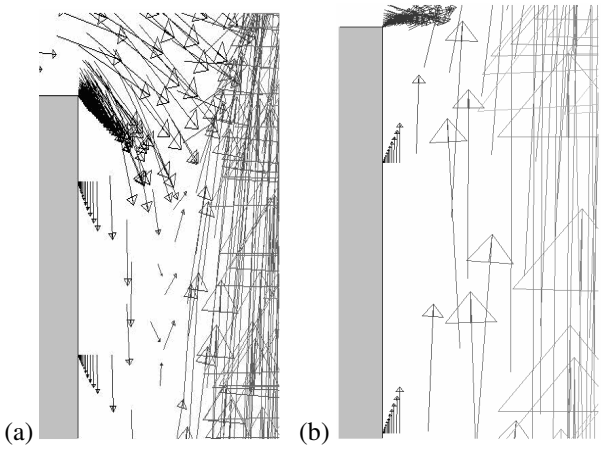


Figure 6. Velocity vectors within the gap near the outer edge of the discs for (a) gap=0.250 mm and (b) gap=0.100 mm at a rotational speed of 1,000 rpm. The pictures show small, approximately 10 μm wide regions, adjacent to the stationary disc.

In Fig. 7 the computed profile of radial velocity is compared with von Karman's solution [8] for a single disc. This velocity profile is presented for the PDD with a gap of 0.250 mm and a rotational speed of 1,000 rpm. The data was taken at a location near the midsection of the lower disc; well before the separated flow region. Since similar agreement was observed for the circumferential velocity component, only the results for the radial component are presented here. As can be seen from the insert of Fig. 7, the agreement is good within the close vicinity of the rotating upper disc. At the same time, at greater distances from the top disc, the computed velocity profile deviates markedly

from von Karman's solution due to the influence of the stationary bottom disc.

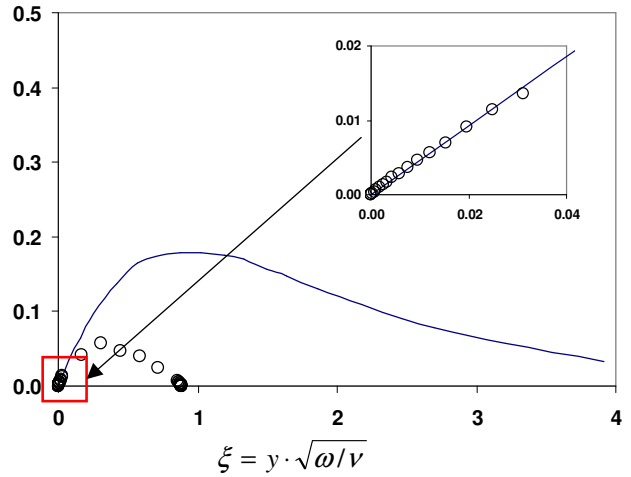


Figure 7. Comparison of computed non-dimensional radial component of velocity (open circles) with von Karman solution (solid line), inside a gap of 0.250 mm and at a rotational speed of 1,000 rpm. The horizontal axis represents a non-dimensional distance $\xi$ from the bottom disc (Y-axis is normal to the disc surface). Insert: profiles within the close vicinity of the rotating disc.

Fig. 8 shows the dependence of computed wall shear stress with distance from the centre of rotation at (a) the bottom surface of the top disc (**red**), (b) the upper surface of the immobile bottom disc (**black**) and (c) the upper surface of the rotating top disc (**green**). Scenario (c) is virtually equivalent to a single rotating disc. The results are presented for both 0.250 mm and 0.100 mm gaps and at rotational speeds of 1,000 and 1,500 rpm. The wall shear stress at the upper surface of the rotating disc is equal to that at the lower surface of the rotating disc as long as the distance from the axis of rotation is less than 20 mm (which is equivalent to the hole in the stationary bottom disc). There is a sudden increase in wall shear stress on the lower surface of the rotating disc in the presence of a stationary disc. However, the wall shear stress on the upper surface of the rotating disc continues to increase with the same trend until instabilities occur as the outer rim of the disc is approached. The differences between the wall shear stress at the rotating disc and the stationary disc decrease as the gap between the discs is reduced. This trend was observed at both rotational speeds.

Figs 5 and 8 also show that flow at a single rotating disc is prone to forming instabilities towards the edges of the disc. The formation of flow instabilities at the wall of a single RD has been noted by other researchers. For example, Poulson [9] proposed that, for a rotating disc electrode, above a critical Re, a central laminar region may be surrounded by transition and turbulent zones where mass transfer will be increasing with increasing radial distance.

The 3-dimensional model of a single RD described above, revealed a similar tendency towards the formation of flow instabilities as shown in Fig. 9. This provides some additional validity for the use of the 2-dimensional axisymmetric model for the PDD.

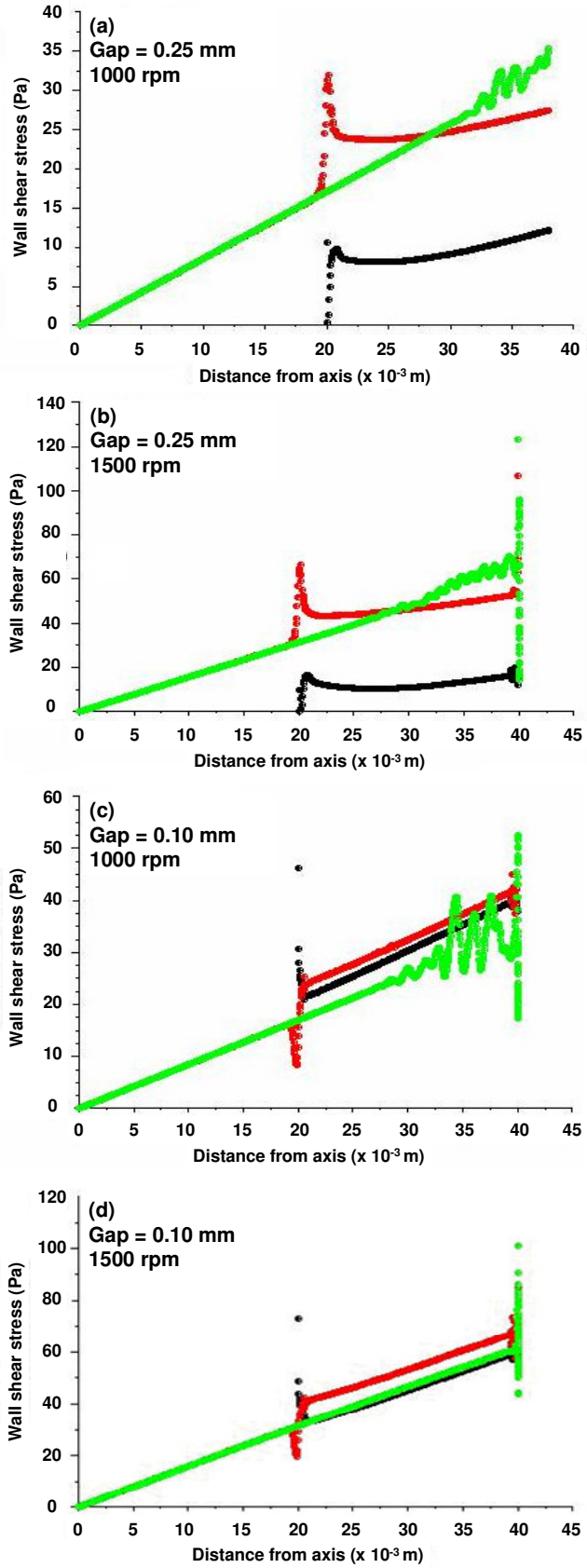


Figure 8. Variation of computed wall shear stress with distance (from the axis of rotation) at the lower surface of rotating top disc (**red**), the upper surface of immobile bottom disc (**black**) and the upper surface of the rotating top disc (**green**) .

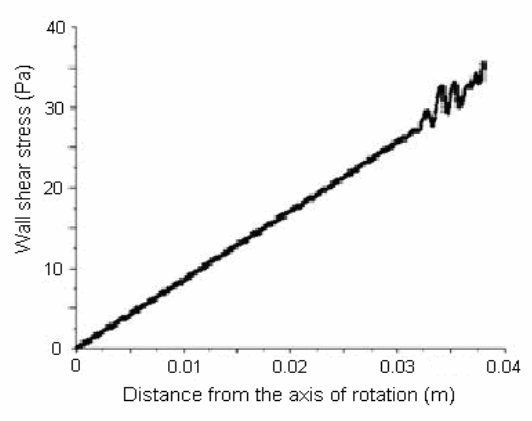


Figure 9. Dependence of computed wall shear stress with distance at the RD (radius = 40 mm, rotation speed = 1,000 rpm) as predicted by the 3-dimensional model.

The CFD model was validated experimentally by measuring the liquid volume flow rates for the PDD as a function of rotation speed at the two gap widths, namely 0.250 mm and 0.100 mm. Fig. 10 compares the CFD data and the experimentally determined values. The volume flow rates were calculated at the exit end of the gap. Agreement is reasonable considering the simplicity of the computational geometry. This provides a fair degree of validity to the 2-dimential axisymmetric CFD model and the data that it generates.

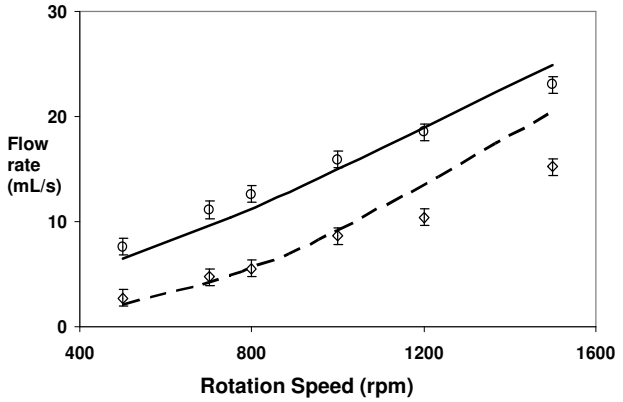


Figure 10. Comparison of computed flow rates (lines) and experimental points (symbols) plotted as a function of rotational speed for gap distances of 0.100 mm (diamonds and dashed line) and 0.250 mm (circles and solid line). Experimental points are averages of 8 readings and the error bars show one standard deviation of mean experimental values.

## Electrochemical Study

To evaluate the performance of the PDD for electrochemical measurements the reduction of dissolved oxygen at the copper electrode has been studied:

$$O_2(aq) + 4e + 2H_2O\ (liq) = 4OH^-(aq)$$

A detailed description of the methodology of this study has been already reported by this group [10]. Here we present the data relevant to the gap widths of 0.100 mm and 0.250 mm.

The PDD working electrode was made from 99.90% copper with an internal diameter of 51 mm and an outer diameter of 74 mm. The same electrochemical system was studied with a copper Rotating Disc Electrode (RDE) of diameter 7 mm, embedded in a cylinder of epoxy resin with an outer diameter of 15 mm.

A selection of "current density - potential" curves at various rotation frequencies for gap distance of 0.100 mm of the PDD are shown in Fig. 11.

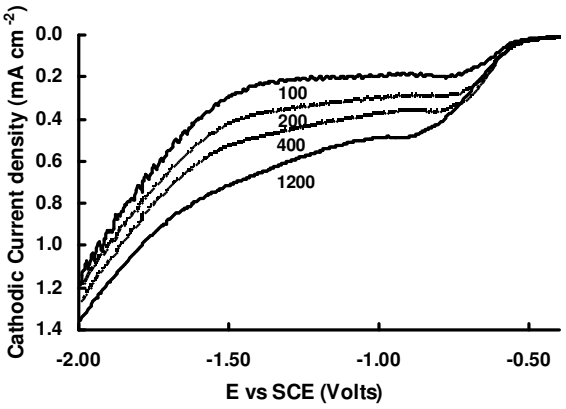


Figure 11. Cathodic "current density - potential" curves for the PDD at selected rotation speeds for the gap distance of 0.100 mm. The potential difference (E) is measured with respect to the saturated calomel electrode (SCE). Rotation speeds (in rpm) are shown for each curve.

The variation of limiting current density with rotation speed for the PDD is provided in Fig. 12 and a similar representation of the data obtained for the RDE is shown in Fig. 13. For both devices the rotation speed was varied over the range 0 to 2,000 rpm.

To thoroughly analyse the presented electrochemical data a CFD model that incorporates the mass transfer of dissolved oxygen is needed. This is an objective of our future studies. At this stage, it is possible only to qualitatively describe the trends observed. Additionally, the comparison of data obtained with different geometries (PDD and RDE) allows us to make some conclusions on the PDD performance.

It is generally accepted that the limiting diffusion current is directly proportional to the mass transfer coefficient and independent of the electrode potential [11]. In turn, the mass transfer coefficient for laminar flow is directly proportional to $U_0^{0.5}$ and inversely proportional to $L^{0.5}$ (where $U_0$ is the bulk flow velocity; and $L$ is the length of diffusion, or, in other words, the dimension of the working electrode measured along the flow direction) [11].

For the purpose of this qualitative analysis it is reasonable to assume that for the PDD the mass-transfer coefficient is determined by the radial velocity component only. The validity of this assumption can be explained as follows. At zero radial velocity, but non-zero circumferential velocity, the mass-transfer of oxygen to the electrode is not possible, since there will be no renewal of liquid at the electrode surface. Hence, after a short time the solution at the electrode surface will be totally depleted of dissolved oxygen. For the RDE delivery of fresh solution to the electrode surface is additionally facilitated by the axial component of the flow velocity, which does not exist in the gap of the PDD. Thus, the trends in the variation of limiting diffusion current seen in both Fig. 12 and Fig. 13 may be interpreted by consideration of the behaviour of both radial and axial velocities for both devices.

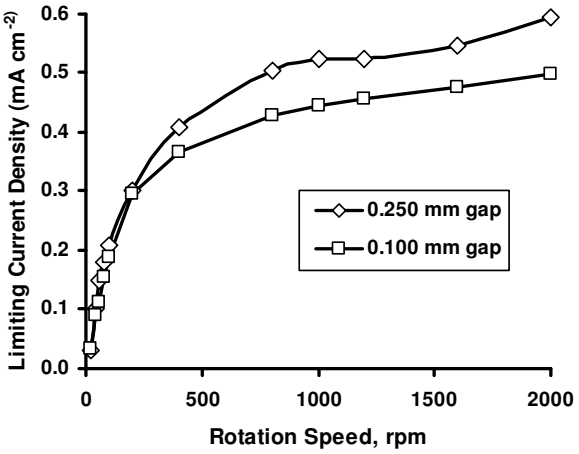


Figure 12. Variation of limiting current density with rotation speed for the PDD with gap widths of 0.100 mm and 0.250 mm.

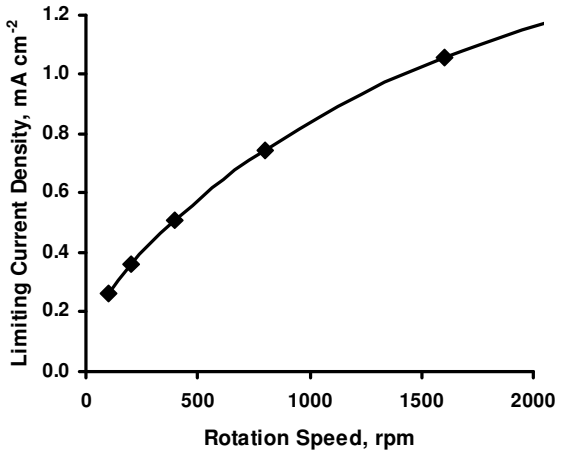


Figure 13. Variation of limiting current density with rotation speed for the RDE.

Fig. 7 shows that the radial velocity within a 0.250 mm gap of the PDD is substantially decreased by the proximity of the immobile disc, compared with radial velocity near the surface of the RDE. For a 0.100 mm gap this decrease is expected to be even more pronounced, since flow rate is lower for the smaller gap (see Fig. 10).

From a comparison of the curves plotted in Figs 12 and 13 it is possible to emphasize the following:

- the values of the limiting current density for the RDE were about two times greater than the relevant values for the PDD,
- the limiting current density curves for the PDD were much steeper in the range of angular velocities from 0 to 400 rpm.

The lower values of the limiting current density for the PDD are likely to be caused by differences in both radial and axial velocities in the vicinity of the working electrode. Another contributing factor is the substantially longer diffusion paths for the PDD (appreciably larger than those for the RDE).

The steepness of the limiting current density curves for the PDD, and the lower values of current density at low rotation speeds, may be attributed to the absence of the axial velocity component near the electrode surface of the PDD. For the PDD fresh solution can be only be delivered to the internal rim of the electrode, while for the RDE there is an axial flux of fresh solution approaching the entire electrode surface.

Higher values of limiting current density observed for a 0.250 mm gap compared to those for a 0.100 mm gap can be easily explained by greater values of the radial velocity within the larger gap. This was experimentally confirmed by the flow rate measurements displayed in Fig. 10. At the same time, the downward trend visible at the right-hand side of the curve for a 0.250 mm gap may be attributable to the occurrence of reversed flow as revealed by the CFD model.

For the RDE the limiting current density is proportional to $\omega^{0.5}$, as long as flow in the device is laminar [11]. To estimate the range of validity of laminar flow at the RDE a simple flow-visualisation experiment was conducted with the RDE cell. Flow was visualised using 50 μm polystyrene particles and light-sheet illumination generated by a laser. It was observed that laminar flow patterns were distorted by the occurrence of vortices when the rotation speed of the RDE exceeded 600 rpm.

At the same time, the CFD model demonstrated that there were no flow instabilities either for 0.100 mm or for 0.250 mm gap between the parallel discs, except for 5 mm long region showing flow at the outlet for a 0.250 mm gap.

The data presented here demonstrated the potential of the PDD as a device capable of generating very high wall shear stresses, while maintaining laminar flow conditions in the gap between discs. From Fig. 8 it can be estimated that the RDE, having a radius of 3.5 mm, can only develop a wall shear stress of 3 Pa at its outer edge at a rotation speed of 1,000 rpm. This is not far removed from the RDE's capabilities of maintaining laminar flow patterns near its surface. At the same time, the wall shear stress at the periphery of the working electrode of the PDD (at the radius of 37 mm) and at a rotation speed of 1,500 rpm was as high as 52 Pa for the gap dimension of 0.100 mm.

## Conclusions

CFD modelling analysis of simplified geometries of both the PDD and the RD has been carried out. Velocity components for the RD compare well with the von Karman solution. For the PDD the velocity components in the gap agreed reasonably well with the von Karman solution at close proximity to the rotating disc. Reverse flow was observed in the gap near the outer edge of the discs of the PDD for a gap distance of 0.250 mm. This flow reversal disappeared as the gap distance was reduced. For the PDD the difference in the wall shear stress at the rotating disc and the stationary disc was reduced as the discs approach each other. The computed volume flow rates of fluid for the PDD agree reasonably well with measured values.

The electrochemical study has confirmed that the PDD has a potential to develop much higher wall shear stresses than the RDE while maintaining laminar flow conditions.

## Acknowledgments

One of us (IMc) gratefully acknowledges financial support from Central Queensland University, the Research Training Support scheme and the Centre for Sustainable Resource Processing. The authors would like to thank R. Clegg for helpful discussions.


## References


[1] Roberge, P., *Erosion-Corrosion*, NACE International, 2004.

[2] ASTM G 170-01a, *Standard Guide for Evaluating and Quantifying Oilfield and Refinery Corrosion Inhibitors in the Laboratory*, ASTM International.

[3] Papavinasam, S., Revie, R. W., Attard, M., Demoz, A. & Michaelian, K., Comparison of laboratory methodologies to evaluate corrosion inhibitors for oil and gas pipelines, *Corrosion*, **59(10)**, 2003, 897-912.

[4] Silvermam, D.C., The Rotating Cylinder Electrode for Examining Velocity-Sensitive Corrosion-A Review, *Corrosion*, **60**, 2004, 1003-1023.

[5] Deev, A., Connor, J.N., Clegg, R., Hoare, G & Druskovich, D., A Rotating Parallel Disc Device for Corrosion Studies, *Corrosion and Prevention Conference Proceedings*, Australasian Corrosion Association, 2005, paper 043.

[6] Tarantseva, K. P.; Pakhomov, V. S. Primenenie sistemy dvuh diskov dlia issledovaniia pittingovoi korrozii stalei v dvizhushchihsia hloridsoderzhashchih sredah (Use of double-disk systems to study pitting corrosion of steel in moving chloride-containing media)**.** *Khimicheskoe i Neftegazovoe Mashinostroenie,* (4), 1997, 74-76.

[7] von Heil, K.. , Heitz, E., Weber, J., Versuchsanlage fuer Werkstoffuntersuchungen bei hohen Stroemungsgeschwindigkeiten (Apparatus for testing materials at high flow speeds)**,** *Materialpruefung*, **23 (5)**, 1981, 166-170.

[8]. von Karman, T., *On Laminar and Turbulent Friction.* Zeitschrift f'ur Angewandte Mathematik und Mechanik, 1921. **1**: p. 233-252.

[9] Poulson, B., Electrochemical measurements in flowing solution, *Corrosion Science*, 1983, 23(4), 391-430.

[10] McNeilly, I.R., Connor, J.N., Deev, A., Clegg, R.,& Druskovich, D., Electrochemical Characterisation of the Parallel Disc Device, *Corrosion and Prevention Conference Proceedings*, Australasian Corrosion Association, 2006, paper 031.

[11] Levich, V. G., Physicochemical Hydrodynamics, Prentice-Hall, Inc.: New Jersey, 1962.